HHS Public Access

Author manuscript

J Allergy Clin Immunol. Author manuscript; available in PMC 2024 July 01.

Published in final edited form as:

J Allergy Clin Immunol. 2023 July ; 152(1): 182–194.e7. doi:10.1016/j.jaci.2023.01.023.

Severe Allergic Dysregulation Due to A Gain of Function Mutation in the Transcription Factor STAT6

Safa Baris, M.D.[1,2,3,*], **Mehdi Benamar, Ph.D.**[4,5,*], **Qian Chen, Ph.D.**[4,5], **Mehmet Cihangir Catak, M.Sc.**[1,2,3], **Mónica Martínez-Blanco, Ph.D.**[4,5], **Muyun Wang, B.A.**[4,5], **Jason Fong, B.Sc.**[4,5], **Michel J. Massaad, Ph.D.**[6,7], **Asena Pinar Sefer, M.D.**[1,2,3], **Altan Kara, Ph.D.**[8], **Royala Babayeva, M.D.**[1,2,3], **Sevgi Bilgic Eltan, M.D.**[1,2,3], **Ayse Deniz Yucelten, M.D.**[9], **Emine Bozkurtlar, M.D.**[10], **Leyla Cinel, M.D.**[10], **Elif Karakoc-Aydiner, M.D.**[1,2,3], **Yumei Zheng, Ph.D.**[11], **Hao Wu, Ph.D.**[11], **Ahmet Ozen, M.D.**[1,2,3], **Klaus Schmitz-Abe, Ph.D.**[4,5,12], **Talal A. Chatila, M.D., M.Sc.**[4,5,13]

[1]Marmara University, School of Medicine, Division of Pediatric Allergy and Immunology, Istanbul, Turkey;

[2]Istanbul Jeffrey Modell Diagnostic and Research Center for Primary Immunodeficiencies, Istanbul, Turkey;

[3]The Isil Berat Barlan Center for Translational Medicine, Istanbul, Turkey;

[4]Division of Immunology, Boston Children's Hospital, Boston, Massachusetts, USA;

[5]Department of Pediatrics, Harvard Medical School, Boston, Massachusetts, USA;

[6]Department of Experimental Pathology, Immunology, and Microbiology, American University of Beirut, Beirut, Lebanon;

[7]Department of Pediatrics and Adolescent Medicine, American University of Beirut Medical Center, Beirut, Lebanon

[8]TUBITAK Marmara Research Center, Gene Engineering and Biotechnology Institute, Gebze, Turkey;

[9]Marmara University, School of Medicine, Department of Dermatology, Istanbul, Turkey;

[10]Marmara University, School of Medicine, Department of Pathology, Istanbul, Turkey;

Corresponding Author: Talal A. Chatila, M.D., M.Sc., Division of Immunology, Boston Children's Hospital, Department of Pediatrics, Harvard Medical School, Boston, MA, USA. talal.chatila@childrens.harvard.edu.

[*]These authors contributed equally

Author Contributions: S.B., M.B. and T.A.C. conceived the project. S.B., A.P.S., R.B., S.B.E., A.D.Y., E.B., L.C., E.K.A. and A.O. carried out the clinical studies. T.A.C. M.B., Q.C., M.C.C., M.M.B., M.W., J.F., and M.M. carried out the signaling, transcriptional and immunological studies. A.K., Y.Z. and H.W. oversaw the structural modeling studies. K.S.A. carried out the whole-exome sequencing analysis. S.B., M.B. and T.A.C. wrote the manuscript.

Conflict of interest disclosure: All authors declare no conflict of interest to disclose.

[11]Department of Biological Chemistry and Molecular Pharmacology, Harvard Medical School, and Program in Cellular and Molecular Medicine, Boston Children's Hospital, Boston, Massachusetts, USA.

[12]The Manton Center for Orphan Disease Research, Boston Children's Hospital, Boston, USA.

[13]Lead Contact

Abstract

Background.—Inborn errors of immunity (IEI) have been implicated in causing immune dysregulation, including allergic diseases. The signal transducer and activator of transcription 6 (STAT6) is a key regulator of allergic responses.

Objective.—We sought to characterize a novel gain-of-function (GOF) STAT6 mutation identified in a child with severe allergic manifestations.

Methods.—We performed whole-exome and targeted gene sequencing, lymphocyte characterization, and molecular and functional analyses of mutated STAT6.

Results.—We report a child with a missense mutation in the DNA binding domain of STAT6 (c.1114G>A, p.E372K) who presented with severe atopic dermatitis, eosinophilia and elevated IgE. Naive lymphocytes from the affected patient displayed increased T_H2 and suppressed T_H1 and T_H17 cell responses. The mutation augmented both basal and cytokine-induced STAT6 phosphorylation without affecting dephosphorylation kinetics. Treatment with the Janus kinase 1/2 inhibitor ruxolitinib reversed STAT6 hyperresponsiveness to IL-4, normalized T_H1, and T_H17, suppressed the eosinophilia and improved the patient's atopic dermatitis.

Conclusions.—We identified a novel IEI due to STAT6 GOF mutation that gave rise to severe allergic dysregulation. Janus kinase inhibitor therapy could represent an effective targeted treatment for this disorder.

Graphical Abstract

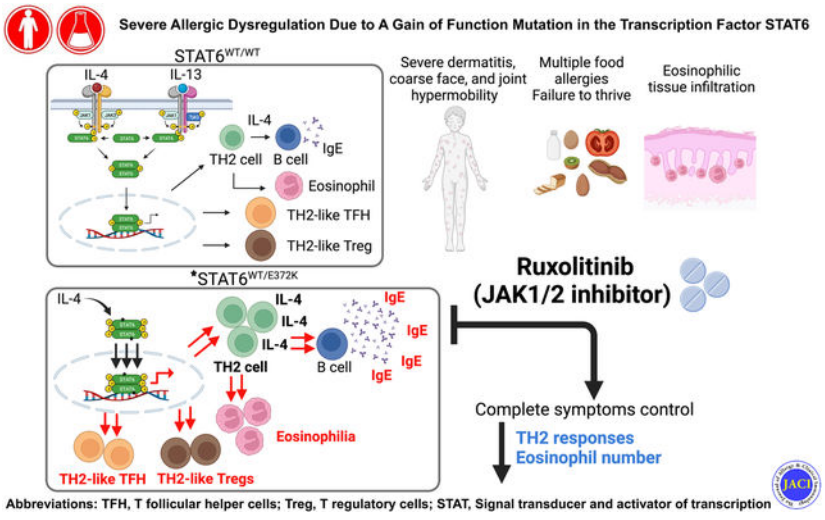

Capsule summary.

Baris et al identify a novel inborn error of immunity disease due to a STAT6 gain of function mutation that results in severe allergic dysregulation and which was effectively managed by Janus kinase inhibitor therapy.

Keywords

Inborn errors of immunity; primary atopic disorders; STAT6; Gain-of-function mutation; Janus Kinase inhibitors; Jakinibs

Introduction

A number of monogenic inborn errors of immunity (IEI) give rise to allergic dysregulation as a prominent disease manifestation[1, 2]. Originally, heterozygous loss-of-function mutations in the signal transducer and activator of transcription 3 (STAT3) were first identified as the cause of autosomal dominant form of the hyper IgE syndrome (HIES)[3]. Afterward, Dedicator of Cytokinesis 8 (DOCK8) deficiency was discovered to cause the autosomal recessive form of the disease[4, 5]. Subsequently, other genetic causes of HIES have been identified, encompassing mutations in *PGM3*, *ZNF341*, *IL6ST*, *IL6R*, *ERBIN*, *TGFBR1*, *TGFBR2* and *CARD11* genes[6–10]. Recently, pertaining to IEI disorders with atypical allergic manifestations, the term of primary atopic disorders was emerged to unify these disorders under one umbrella[9, 11], encompassing more than 35 monogenetic disorders[2, 8]. Gain-of-function (GOF) mutations in Janus kinase (JAK)-STAT signaling pathways have also been associated with atopic manifestations[12], including ones targeting *STAT3*, *STAT5B* and *JAK1*[13–16].

STAT6 is the central transcription factor that mediates the biological effects of interleukin 4 (IL-4) and IL-13[17–19]. The binding of IL-4 and IL-13 to IL-4R complexes triggers the phosphorylation of conserved tyrosine residues in the cytoplasmic domain of the common IL-4 receptor alpha (IL-4Rα) subunit by the receptor-associated JAK kinases[20, 21]. STAT6 is subsequently recruited through the binding of its tandem Src homology 2 (SH2) domains to the IL-4Rα phosphotyrosine docking sites[22]. Once bound to the receptor, STAT6 is phosphorylated by the JAK kinases, resulting in its dimerization via the SH2 domains and its translocation into the nucleus, where it activates the expression of target genes by binding to a specific DNA sequence motif[23, 24].

The IL-4R-STAT6 axis plays a critical role in type 2 immunity, directing protective responses to parasites and toxins, promoting B cell development, activation and class switching to IgE and IgG1, and directing overall tissue repair[22, 25, 26]. By the same token, its dysregulation plays a pathogenic role in different allergic diseases[27]. STAT6 signaling promotes the differentiation of T helper type 2 (T_H2) cells by upregulating the expression of the master transcriptional regulator GATA binding protein 3 (GATA3)[28, 29]. Furthermore, STAT6 signaling renders T_H2 cells resistant to regulatory T (Treg) cell-mediated suppression[30], while excessive STAT6 signaling in Treg cells results in their acquisition of a T_H2 cell-like phenotype that contributes to the allergic response[31]. STAT6 single nucleotide polymorphisms are associated with increased serum IgE, eosinophil, food allergy, and asthma[32, 33]. Exaggerated STAT6 activity due to somatic *STAT6* mutations

is often linked to malignancies, especially Hodgkin and non-Hodgkin lymphomas[34, 35]. A transgenic mouse model (STAT6VT) expressing a lymphoid tissue-restricted constitutively active STAT6 GOF variant created by introducing mutations in the SH2 domains exhibited IL-4-independent augmented T_H2-cell response. These mice developed atopic dermatitis (AD)-like phenotype with blepharitis and allergic lung inflammation[36, 37]. In line with the known critical function of IL-4R-STAT6 axis in the initiation and promotion of T_H2 responses, we herein report a patient with germline sporadic GOF mutation in *STAT6* as the molecular etiology of a previously unknown syndromic HIES. We showcase the impact of perturbations in T-cell responses downstream of altered STAT6 signaling and deliver a proof-of-concept for improving immune cell activation and differentiation in patient cells by Janus Kinase inhibitors (Jakinibs).

Materials and Methods

Clinical assessments.

The local ethics committee from Marmara University and Boston Children's Hospital approved the clinical and research studies protocol and written informed consent was obtained from the family. We documented the clinical and demographic features of the patient and provided data regarding long-term follow-up.

Antibodies and flow cytometry.

To determine detailed lymphocyte subsets, the following monoclonal antibodies (mAbs) were used: Fluorescein isothiocyanate (FITC)-conjugated CD3 (UCHT1, BC, FRA), Allophycocyanin (APC)-Alexa Fluor 700 (APC-A700) CD4 (13B8.2, BC), Krome Orange (KO) CD45 (J33, BC), Alexa Fluor 750 (APC-A750) CD45RA (2H4DH11LDB9, BC), Phycoerythrin-Cyanin 7 (PC7) CD8 (SFCI21Thy2D3, BC), Phycoerythrin-Texas Red-x (ECD) CD45RO (UCHL1, BC), PC5.5 CD25 (B1.49.9, BC), Alexa Fluor 647 Foxp3 (259D, BD Biosciences, Calif, USA), PE P-STAT6 (A15137E, Biolegend), FITC "Chemoattractant receptor homologous molecule expressed on TH2-type cells" (CRTH2) (BM16, Biolegend), APC-GATA binding protein 3 (GATA3) (16E10A23, Biolegend), BV605 CCR4 (L291H4, Biolegend), PE RORγt (Q31–378, BD Biosciences), CD27 (0323, Biolegend), CD19 (4G7, Biolegend), CD23 (EBVCS-5, Biolegend), IgE (MHE-18, Biolegend), IgD (IA6–2, Biolegend), CD38 (HB-7, Biolegend), CD20 (2H7, Biolegend). Peripheral blood lymphocyte subset analyses, upregulation, and proliferation assays were performed by flow cytometry as described previously[38–40]. For lymphocyte subset analysis, 100μl of whole blood was incubated with mAbs against surface markers for 20 minutes in the dark at room temperature. Red cells were lysed and washed before acquisition. For Treg cells visualization, after isolation of peripheral blood mononuclear cells (PBMCs), the cells were fixated and permeabilized, followed by overnight incubation for intracellular Foxp3 staining. All stained cells were acquired with a Navios EX cytometer (Beckman Coulter) and analyzed with Kaluza Analysis Software (Version 2.1). CD25 upregulation and proliferation assay were performed by isolation of peripheral blood mononuclear cells and stimulation in anti-CD3/anti-CD28 (1μg/ml each) 96-well plates for 3 days, following labeling with CellTrace Violet (Thermo Fisher) according to manufacturer's instructions. CD69 upregulation was evaluated after 24 hours of stimulation with anti-CD3/anti-CD28

(1μg/ml each). For intracellular IL-4, IL-17A, IL-10 and IFN-γ detection, cell suspensions (1×10^6 cells) were incubated with protein transport inhibitor containing monensin (BD Bioscience, USA), PMA (50 ng/ml) and ionomycin (1 μg/ml) for 6 hours. After incubation, cells were fixed. For intracellular cytokine staining, fixed cell pellets were resuspended in permeabilization reagent containing saponin (Thermo Fisher Scientific, USA), mixed with fluorescent-labeled cytokine specific antibody. After 45 minutes of incubation, cells were washed twice and cell surface staining was performed with fluorescent-labeled antibodies against CD4, CD45RA and CD45RO. Stained cells were acquired by Navios EX cytometer (Beckman Coulter) and analyzed by FlowJo software (TreeStar, Ashland, Ore).

Analysis of phosho(p)-STATs by phosphoflow.

Total PBMCs from either Healthy controls or Patient pre and post-treatment were stimulated at 37°C in non-supplemented RPMI 1640 with IL-4 (20 ng/ml), IL-2 (10 ng/ml) or IL-6 (20 ng/ml). For the STAT6 dephosphorylation following cytokine withdrawal, cells were washed with RPMI after stimulation with IL-4 and incubated in RPMI at 37°C and examined for p-STAT6 levels at 0 to 30 min, as previously described for STAT1 GOF mutations[41, 42]. Reactions were stopped and cells were permeabilized using a Foxp3/transcription factor staining buffer (eBiosciences) and Perm buffer III (BD Biosciences). Cells were stained using PE anti pY641-STAT6 (A15137E, Biolegend), APC anti-pY694-STAT5 (A17016B.Rec, Biolegend), Efluor450 Foxp3 (236A/E7, ThermoFischer), APC-Cy7 CD3 (OKT3, Biolegend), BV785 CD4 (OKT4, Biolegend), and/or BV605 CD8 (HIT8a, Biolegend) mAbs. Samples were acquired on a Fortessa cytometer (BD) and data were analyzed using the FlowJo software.

In vitro B cell IgE class switching assay.

$CD19^+IgD^+CD27^-CD23^-IgE^-$ naïve B cells were purified by fluorescent-activated cell sorting (FACS) and cultured *in vitro* for 4 days at 30,000 cells/tissue culture plate well in the presence of either an IgG1 isotype control antibody (Biolegend, Cat# 400165, 0.5μg/ml) or with an anti-CD40 mAb (0.5μg/ml, Biolegend, Cat# 334350, 0.5μg/ml)+IL-4 (20ng/ml, Peprotech). At the end of the culture period the cells were stained with a viability dye and anti-CD19,-CD27, -CD23 and-IgE mAbs and analyzed by flow cytometry.

ELISA for human total IgE.

The levels of IgE in cells supernatants were determined by Sandwich ELISA. 96-well plates were coated with 2 μg/well of Purified Mouse Anti-Human IgE (BD Biosciences). For the standard curve Chimeric Human IgE anti NP (Bio-Rad) was used. The supernatants were incubated at 4°C overnight, followed by a detection antibody incubation step with Goat anti-Human IgE Fc Secondary Antibody, HRP (ThermoFisher Scientific). The reaction was developed using TMB as substrate (Thermo Scientific) and read at 450 nm.

Generation of STAT6 variant plasmids and expression of STAT6 variants.

A plasmid used for transfection studies contained full-length STAT6 in a pCMV6 entry vector with a C-terminal GFP tag (pCMV6-AC-STAT6-GFP) which was purchased from OriGene (RG210065). The directed STAT6 mutagenesis (c.G1114A; p.E372K) plasmid

was generated with standard cloning techniques by using pCMV6-AC-STAT6-GFP as a template. Transient expression of STAT6 variants in HEK293T cells were accomplished using GeneJuice transfection reagent (Merck Millipore) according to manufacturer's recommendations. Briefly, the day before transfection, HEK293T cells were seeded at a density of 5×10^5 cells per well in 6 well plates in 3ml Dulbecco modified Eagle medium (DMEM) with 10% FBS (Gibco, Life Technologies; Rockville, MD, USA) and incubated for 24 hours at 37°C. The next day, HEK293T cells were transiently transfected with 2ug of either pCMV6-AC-STAT6-GFP wild type or STAT6 mutant plasmid using GeneJuice transfection reagent. Cells were harvested after 24h after transfection for phospho-flow cytometry analysis.

Luciferase reporter assays.

The p4xSTAT6-Luc2P luciferase reporter plasmid encoding 4xSTAT6 binding sites [TTCCCAAGAA] was obtained from Addgene (catalogue no. 35554) and used to assess STAT6 promoter activity. The pRL-SV40 Renilla luciferase control reporter vector was obtained from Promega (catalogue no. E2261) and was used in co-transfection studies with p4xSTAT6-Luc2P for internal normalization. HEK293 cells were seeded in 96-well plates overnight at a density of 30,000 cells per well and transfected with 20ng of plasmids encoding either GFP-tagged WT or p.E372K STAT6. The cells were further transfected with 100ng of p4xSTAT6-Luc2P and 4ng the pRL-SV40 vectors using Fugene HD transfection reagent (Promega, catalogue no. E2311), according to manufacturer's recommendations. The next day, transfected cells were stimulated with 100ng/mL of IL-4 (PeproTech, catalogue no. 200–04), and transfected but otherwise untreated cells were used as a control group. Firefly and Renilla luciferase activities, as indicated by relative luminescence units (RLU), were determined using Dual-Glo luciferase assay kits (Promega, catalogue no. E2920), according to the manufacturer's instructions. Luciferase activity was measured on BioTek Synergy HTX Multi-Mode Microplate Reader.

Immunofluorescence imaging.

Confocal microscopic analysis of STAT6 and p-STAT6 nuclear translocation was carried out following previously described methods[43]. HEK293T cells were grown on the coverslips and transfected with indicated plasmid. After stimulation with 100ng/mL of IL-4 for 1 and 4h, the cells were fixed for 20 min in 4% paraformaldehyde and permeabilized with 0.3% Triton X-100. After blocked with 5% bovine serum albumin, the cells were stained with a mouse anti-p-STAT6 mAb [clone 4H253, Santa Cruz Biotechnology, catalogue number sc71793) and anti-STAT6 rabbit mAb (clone D3H4, Cell signaling, catalogue number 5397), incubated at 4 °C overnight. Alexa Fluor 555-goat anti-mouse IgG1 (Invitrogen, catalogue number A21127) and Alexa Fluor Plus-647 conjugated goat anti-rabbit (Invitrogen, catalogue number A32733) secondary antibodies (1:500 dilution) were used for visualizing. After, cells were washed with PBS and stained with 4,6-diamidino-2-phenylindole (DAPI) (Sigma; 1:10,000 dilution). Images were acquired with a Zeiss LSM880 confocal microscope and ZEN imaging software. Ten fields were selected randomly and total cells in the field were analyzed for the percentage of STAT6 nuclear localization using ImageJ software.

Whole exome sequencing.

The genetic diagnosis was made by whole-exome sequencing (WES) and the detected variant was confirmed by Sanger sequencing. Briefly, genomic DNA was extracted from peripheral blood samples and 1μg of DNA was used for exome capture using the IDT XGen exome target design or Agilent SureSelect Human All Exon. Generated libraries were sequenced using 75 bp paired-end sequencing on an Illumina NovaSeq-6000 and BGISeq-500 platform. Captured fragments were sequenced to achieve a minimum of 85% of the target bases covered at 20x or greater coverage. Analysis of WES data was performed using "Variant Explorer Pipeline" (VExP) to narrow down potential candidate variants[44]. Raw data were processed, filtered and analyzed according VExP recommendations. Candidate genes were further evaluated by our research team (Table E1 in the Online Repository). Sanger sequencing was performed to confirm the mutation identified by the WES. Briefly, genomic DNA was amplified by a polymerase chain reaction and amplimers were sequenced using the Big Dye Terminator v1.1 Cycle Sequencing Kit (Applied Biosystems; Life Technologies, Darmstadt, Germany) on an Applied Biosystems 3130 Genetic Analyzer.

Statistical analysis.

The data expressed as mean and standard error of mean (SEM). Analysis of luciferase reporter activity, p-STAT6 phosphorylation and p-STAT6 nuclear translocation in HEK293 cells was carried out using 2-way ANOVA with post-test analysis. Differences in values were considered significant at a p value <0.05.

Results

Identification of a novel STAT6 mutation (STAT6^{E372K}) causing severe allergy dysregulation.

The index case is a ten-year-old boy born to consanguineous parents. He presented in the newborn period with severe atopic eczema, incessant itching, severe growth retardation, generalized lymphadenopathy, and pneumonia. He had generalized skin rash since the newborn period and itching was severely affecting his quality of life. Eczema and itching did not benefit from any local therapies and oral antihistamines. The eczema was associated with a robust IgE response to aero-and food allergens, including high levels of specific serum IgE to mite, grass, wheat, soy, cow milk, egg, tomato, kiwi, almond, and nuts. He experienced urticaria after ingestion of kiwi, and almond, and displayed dysphagia with vomiting following intake of wheat products, egg white, and tomato. A skin biopsy was performed at the age of seven years, which revealed chronic dermal inflammation characterized by perivascular and perifollicular eosinophils, follicular mucinosis, and fibrosis (Fig. 1A). During this period, the patient developed generalized lymphadenopathy involving the cervical, axillary, and inguinal lymph node, which persisted despite antibiotic therapy, prompting screening for malignancy. A bone marrow aspirate and biopsy were normal. An inguinal lymph node biopsy revealed findings consistent with reactive follicular hyperplasia, and paracortical enlargement. Meanwhile, he developed fever and painful swellings in his skin and axillary lymph nodes, and an ultrasound detected a

local tissue abscess. *Staphylococcus aureus* was isolated and was treated with a systemic anti-staphylococcal antibiotic regimen.

One year later, he was admitted to the hospital with a fever, and cough. Chest X-ray showed pneumonia and parapneumonic effusion. Methicillin resistance *Staphylococcus aureus* was detected in his sputum and blood cultures. Lung computed tomography revealed ground-glass densities and interlobular septal thickenings, predominantly in the peripheral and paramediastinal parts of both lungs. On physical examination, his weight (18 kg) and height (118 cm) were below the 3rd percentile and he had mild developmental delay. There were xerotic excoriated lichenified eczematous lesions covering all the body, accompanied by hyperpigmentation. Coarse facial appearance with broad nasal bridge, increased alar width, and deep-set eyes, mild high palate arch, hyperextensibility, digital clubbing, and enlarged cervical, axillary and inguinal lymph nodes were also notable. He had normal dentition but with enamel hypoplasia (Fig. E1 in the Online Repository). The scoring of AD (SCORAD) and National Institute of Health-HIES scores were 96 and 44; respectively[45, 46] (Table E2 in the Online Repository). Nevertheless, he had no evidence of AD-HIES-associated pneumotocele formation or vascular anomalies as evidenced by normal lung computed tomography, brain magnetic resonance imaging, and angiography. He was commenced on prophylactic antibiotic therapy and intravenous immunoglobulin replacement. Due to difficulty in swallowing, we performed upper and lower gastrointestinal endoscopy and showed findings of esophagitis and colitis with mild eosinophilic infiltrations (Fig. 1A). The endocrinologic evaluation revealed growth hormone (GH) deficiency (GH: 0.93 mIU/L (5.4–10.3), IGF-1: 72 ug/L (85.7–343)), and he was scheduled to start GH replacement therapy. His immunological workup was particularly notable for persistent eosinophilia (3,100/mm^3). He had normal serum IgG, IgA, and IgM levels but high IgE (44,226 IU/ml), and protective protein antigen IgG responses, and IgM responses to isohemagglutinins. He had increased CD3$^+$ and CD3$^+$CD4$^+$ T counts with a predominance of effector memory CD4$^+$ T cells in the flow cytometric analysis (Table 1). T-cell proliferation with anti-CD3/anti-CD28 antibodies and phytohemagglutinin (PHA), and upregulation of CD25 and CD69 were normal in the patient when compared with the healthy controls (Fig. E2 in the Online Repository).

Identification of pathogenic STAT6 variant.

WES analysis revealed a novel heterozygous G>A substitution in exon 22 of *STAT6* gene (c.1114G>A, p.E372K; based on STAT6 isoform 1, NM_003153.5) (Table E1 in the Online Repository). This mutation, which mapped to the DNA binding domain (DBD) of STAT6 and was confirmed by Sanger sequencing, has not been previously reported in the genomAD, ExAC, dbSNP, or 1000 Genomes Project databases, and it involved an amino acid residue that is conserved among species (Fig. 1B–D). Interestingly, this variant was previously identified in the COSMIC (Catalog of somatic mutations in cancer) database as a somatic mutation associated with lymphoid malignancies[47]. It was not detected in DNA sequences of other available family members, including the mother and siblings, suggesting that it was sporadic. The deleteriousness of the variant was suggested by a high Combined Annotation Dependent Depletion (CADD) score of 27.9. The *in-silico* pathogenicity scores of SIFT, REVEL, Mutation tester, and PROVEAN were also damaging. The mutation was

predicted to minimally affect protein stability as evaluated in silico by PremPS (Fig. E3A in the Online Repository)[48]. Multiple sequence alignment analysis of STAT6 with other STAT proteins produced by ClusterW and ESpript (espript.ibcp.fr/ESPript/ESPript/) showed that the $STAT6^{E372K}$ variant equivalent of $STAT3^{N420K}$, which has been reported as GOF in the literature (Fig. E3B in the Online Repository)[49, 50]. Locating within the DNA-interacting loop, the $STAT6^{E372K}$ variant is homologous to $STAT3^{N420K}$ GOF mutants. Similar to $STAT3^{N420K}$, $STAT6^{E372K}$ also features an elongated side chain comparing to wild type (Fig. 1E, F). Such extension increases the possibility of additional protein-DNA contact. Moreover, change of the side charge from neutral ($STAT3^{N420K}$) or negative ($STAT6^{E372K}$) to positive is likely to enable the interactions to the negatively charged DNA phosphate groups. Overall, these analyses suggested that the $STAT6^{E372K}$ variant is deleterious and may act as GOF mutation.

The $STAT6^{E372K}$ mutation is associated with dysregulated T_H2 cell responses.

Based on the role of STAT6 in T_H2 cell responses, we analyzed circulating $CD4^+$ T-cell subtypes including naïve, memory, T_H1, T_H2, T_H17, Treg, and circulating follicular helper T (cT_{FH}) cells. The gating strategy is presented in Fig. E4. The patient with the $STAT6^{E372K}$ variant exhibited an increased frequency of circulating memory $CD4^+$ T cells ($CD3^+CD4^+CD45RA^-$ $CD45RO^+$) and a decreased frequency of circulating naïve $CD4^+$ T cells ($CD3^+CD4^+CD45RA^+CD45RO^-$) (Fig. 2A). More detailed analysis of the $CD4^+$ T cells compartment revealed that the patient with the $STAT6^{E372K}$ variant had an increase of T_H2 $CD4^+$ T cells as reflected by the expression of the T_H2 cell markers GATA3, CRTH2 and CCR4 ($CD3^+CD4^+GATA3^+$, $CD3^+CD4^+CRTH2^+$ and $CD3^+CD4^+CCR4^+$). There was also a trend towards decreased expression of T_H1 ($CD3^+CD4^+CXCR3^+$) and T_H17 ($CD3^+CD4^+ROR\gamma T$, $CD3^+CD4^+CCR6^+$) cell markers (Fig. 2B, C). Treg cell analysis also revealed an increase of T_H2 skewed Treg cells[31], indicative of their T_H2 cell-like reprogramming ($CD3^+CD4^+CD127^-Foxp3^+GATA3^+$, $CD3^+CD4^+CD127^-Foxp3^+CRTH2^+$ and $CD3^+CD4^+CD127^-Foxp3^+CCR4^+$) and a decrease of T_H1 ($CD3^+CD4^+CD127^-Foxp3^+CXCR3^+$) and T_H17 ($CD3^+CD4^+CD127^-Foxp3^+ROR\gamma t^+$, $CD3^+CD4^+CD127^-Foxp3^+CCR6^+$) Treg cells (Fig. 2D, E). Further analysis also revealed a decrease of cT_{FH} ($CD4^+CXCR5^+PD1^+$) cells, skewing of these cells toward a T_H2 phenotype ($CD4^+CXCR5^+CD45RA^-CXCR3^-CCR6^-$) and away from other T_{FH} cell phenotypes including $T_{FH}1$-like ($CD4^+CXCR5^+CD45RA^-CXCR3^+CCR6^-$) and $T_{FH}17$-like ($CD4^+CXCR5^+CD45RA^-CXCR3^-CCR6^+$) (Fig. 2F). There was also an increase in circulating T follicular regulatory T cells (cT_{FR}) ($CD4^+CXCR5^+PD1^+CD127^-Foxp3^+$) (Fig. 2F).

The $STAT6^{E372K}$ mutation is associated with enhanced B cell switching to IgE.

Analysis of patient peripheral blood B cells revealed a similar frequency of $CD19^+CD27^+IgD^-$ class switched memory B cells but increased frequency of circulating $CD19^+CD20^-CD38^+$ plasmablasts relative to control subjects (Fig. 3A,B, C). In particular, there was a high frequency of circulating $CD19^+CD27^+IgE^+$ B cells in patient relative to controls (Fig. 3D). This increase reflected in part heightened expression on circulating patient B cells of the IL-4-inducible low affinity IgE receptor (CD23) (Fig. 3E)[51], which could then bind circulating IgE regardless of the status of the B cell class switch isotype.

Further analysis revealed that a subset of circulating B cells that do not express CD23 still exhibited IgE staining, raising the possibility of enhanced switching to IgE (Fig. 3F).

To determine the propensity of patient B cells to switch to IgE, we sorted naïve B cells ($CD19^+IgD^+CD27^-CD23^-IgE^-$) to high purity (≥97%) following a gating strategy outlined in (Fig. 4A, B). The cells were cultured in vitro and stimulated with anti-CD40 mAb+IL-4 to induce switching to IgE[52]. Results showed that the patient B cells exhibited markedly increased IgE staining and total IgE in the supernatants at the end of the culture, indicative of enhanced switching to IgE (Fig. 4C, D)

$STAT6^{E372K}$ is a GOF mutation.

Analysis of primary $CD4^+$ T cells revealed a modest increase in the expression of STAT6 in the patient relative to controls (Fig. 5A). To further characterize the functional significance of this mutation, primary T cells were stimulated with IL-4 for 5 to 30-minutes, and analysis by phosphoflow revealed that the $STAT6^{E372K}$ mutation induces hyper-phosphorylation of STAT6 which was evidenced at baseline and increased dramatically post-IL-4 stimulation (Fig. 5B).

Stimulation with IL-2 or IL-6 resulted in similar levels of STAT5 and STAT3 phosphorylation, respectively, in patient and control T cells (Fig. 5C). The $STAT6^{E372K}$ mutation did not appear to delay the STAT6 dephosphorylation upon cytokine deprivation as evidenced by a rapid p-STAT6 decline, indicating that its main effect is to enhance the phosphorylation of STAT6 by the JAK kinases (Fig. 3D).

To further assess the impact of this mutation on STAT6 activity, we transfected HEK293 cells with either $STAT6^{E372K}$ or control $STAT6^{WT}$ expression plasmids and analyzed STAT6 protein expression and p-STAT6 formation in response to IL-4 treatment. Flow cytometric analysis revealed that the $STAT6^{E372K}$ mutation did not impact STAT6 protein expression in HEK293 (Fig. 5E). To analyze the role of this mutation on the STAT6 activation, Phosphoflow analysis revealed that treatment of the respectively transfected cells with IL-4 resulted in increased phosphorylation of the $STAT6^{E372K}$ mutant compared to $STAT6^{WT}$ (Fig. 5F). This increase persisted when the phosphoflow staining was normalized for STAT6 expression. We further analyzed the capacity of the $STAT6^{E372K}$ mutant to upregulate STAT6-dependent gene expression compared to $STAT6^{WT}$ by co-transfecting HEK293 cells with a luciferase gene driven by STAT6 response elements together with the respective STAT6 expressing construct. Results showed that the $STAT6^{E372K}$ mutant drove higher expression of the luciferase gene early (1 hr) compared to $STAT6^{WT}$, but that this increase was tempered at later time points (Fig. 5G). We also analyzed the nuclear translocation of p-STAT6 species in HEK293 cells that were transfected with either $STAT6^{WT}$ or the $STAT6^{E372K}$ mutant and then stimulated with IL-4. The p-$STAT6^{E372K}$ mutant exhibited a modest increase in nuclear translocation at baseline relative to p-$STAT6^{WT}$. IL-4 treatment resulted in progressive nuclear translocation of p-STAT6 over the 4 hr duration of the study that was markedly increased for p-$STAT6^{E372K}$ mutant relative to p-$STAT6^{WT}$ (Fig. 5H) Overall, these results demonstrated that the $STAT6^{E372K}$ is a GOF mutation that upregulates phosphorylation and the nuclear translocation of STAT6.

Ruxolitinib therapy suppresses the allergic dysregulation caused by STAT6^{E372K}.

Based on the immunological studies showing STAT6^{E372K} as a GOF mutation, and in view of the success of Jakinib therapy in patient with STAT GOF mutations, we initiated therapy of our patient with oral ruxolitinib (10 mg/m^2/dose, twice daily). Ruxolitinib rapidly controlled the skin disease with decreased itching noticed within three days of therapy. The SCORAD levels decreased from 96 to 25, and ruxolitinib therapy induced almost normal skin hydration and appearance at one month post therapy (Fig. 6A). A normalization in blood eosinophil number and decrease in serum IgE levels were noticed (Table 1). Ruxolitinib therapy was not associated with drug-related adverse effects or infections. Currently, he continues to do well after six months of therapy with a most recent SCORAD of 8. Furthermore, there was resolution of his eosinophilic esophagitis-associated dysphagia and a catch-up in his weight from 18 kg (≤3rd percentile) to 24 kg (3rd percentile). Immunological studies carried out at one month post initiation of therapy revealed decreased frequencies of circulating memory T cells and an increase in those of naïve T cells (Fig. 6B). A reduction of the T_H2 skewing was also noted (Fig. 6C, D), associated with an increased T_H1 and T_H17 cell frequencies (Fig. 6E, F). The percentage of IL-4 producing circulating CD4$^+$ T cells, which was increased in the patient pre-ruxolitinib, declined on therapy, while those of other T_H1 and T_H17 cell subsets increased (Fig. 6G, H). Ruxolitinib treatment did not impact T_{FH} cell frequencies or their T_H2-like skewing but normalized the frequencies of circulating Treg and T_{FR} cells (Fig. E5 in the Online Repository). Ruxolitinib treatment did not affect the upregulation of activation markers including CD69 and CD25 following in vitro T cell activation nor did it impact T cell proliferation in response to stimulation with T cell mitogens including anti-CD3+anti-CD28 antibodies and PHA (Fig. E1). Finally, treatment with ruxolitinib normalized p-STAT6 induction in patient T cells both at baseline and in response to cytokine treatment (IL-4) (Fig.6I). These results indicated that treatment with the JAK1 inhibitor ruxolitinib effectively suppressed the clinical and immunological attributes of the allergic dysregulation associated with STAT6^{E372K} mutation.

Discussion

In this study, we describe the identification of a STAT6^{E372K} GOF mutation in a child with allergic dysregulation characterized by early-onset severe AD accompanied by features mimicking HIES syndrome. The mutation resulted in increased STAT6 activation as evidenced by increased phospho-STAT6 both at baseline and following IL-4-treatment and accelerated p-STAT6 translocation to the nucleus. STAT6-dependent reporter gene activation was increased early (1hr) but not later (4 hr) post IL-4 activation, which may reflect increased p-STAT6 sequestration in the nucleus. These alterations in STAT6 activity were associated with enhanced T_H2 cell responses and augmented B cell isotype switching to IgE. Furthermore, the dysregulated STAT6 activity was associated with T_H2 cell-like skewing of Treg cells, a phenotype conducive to immune dysregulation and exacerbated allergic inflammation[31]. The capacity of ruxolitinib to suppress the STAT6^{E372K} hyperactivity and ameliorate disease manifestation identify Jakinib inhibitors as appropriate targeted therapy in this novel disorder.

STAT6 is a central transcription factor in the nexus of type 2 immunity by virtue of its activation by IL-4 and IL-13 to promote a variety of allergic responses including T_H2 cell differentiation[53], B cell activation and IgE production[22, 25], alternate macrophage and epithelial goblet cell differentiation and innate lymphoid cells type 2 (ILC2), mast cells activation[54–57]. As such, its dysregulation would be predicted to precipitate a broad allergic inflammatory response, as is reflected in the development in our patient of severe atopic dermatitis, eosinophilic esophagitis, food allergy and hyper IgE[58]. Some of these phenotypes were reflected in related transgenic mouse models of enhanced STAT6 signaling. The first is an engineered STAT6 mutant with two alanine substitutions in the SH2 domain (STAT6VT), whose expression is restricted to lymphoid tissues. The STAT6VT mice develop marked T_H2-cell skewing, severe atopic dermatitis (AD)-like phenotype with blepharitis and allergic lung inflammation[36, 37]. In a second model, an inactivating mutation (IL-4RαY709→F) was engineered in the immunotyrosine inhibitory motif (ITIM) in the cytoplasmic domain of the IL-4Rα chain, which dampens STAT6 activation by recruiting the phosphotyrosine phosphatase Shp1[59]. Accordingly, the mutant receptor mediated enhanced IL-4- and IL-13-induced STAT6 phosphorylation and activation[57, 59]. These mice exhibited augmented allergic responses including allergic airway inflammation and food allergy in part by a mechanism involving the Th2 cell like reprogramming of their Treg cells, leading to their failure to effectively control allergic responses[31, 60, 61]. Of note, STAT6VT T effector cells also appear resistant to Treg cell-mediated suppression[30]. Consistent with the T_H2 cell like phenotype of the Treg cells of the patient reported herein, one can postulate that the aberrant $STAT6^{E372K}$ may similarly act in part to impair Treg cell control of the allergic response, giving rise among other things of dysregulated T_H2 and $PD1^+$ T_H2-like cT_{FH} cell responses to drive the allergic inflammation in our patient.

Somatic GOF mutations in STAT6, including $STAT6^{E372K}$, have been previously described in follicular lymphomas. However, in that report, the E372K mutation was found associated with largely autonomous transcriptional activity independent of IL-4 or STAT6-Y641 phosphorylation[34]. In contrast, our own studies showed that the GOF attributes of the $STAT6^{E372K}$ mutation were overwhelmingly IL-4 dependent in terms of p-STAT6 formation, nuclear translocation and luciferase reporter activation as well as B cell switching to IgE. Furthermore, our patient responded to ruxolitinib, indicative of IL-4 receptor-driven $STAT6^{E372}$ activation in the patient. These differences may reflect the methods employed in the respective studies.

The identification of a germline GOF mutation in STAT6 expands the spectrum of GOF mutations in JAK-STAT pathways. In these disorders, the JAK inhibitors are leveraged to control of JAK-STAT pathway and consequently control different disease activities[62]. Recently, data are available on the successful usage of JAK inhibitors in IEI disorders like STAT1, STAT3, STAT5B, and JAK1 GOFs, interferonopathies, and SOCS1 haploinsufficiency[15, 42, 63–66]. We previously showed that treatment with the JAK inhibitor in patients with STAT1 GOF mutations decreased hyperresponsiveness to type I and II interferons, normalized T_H1 and follicular T helper cell responses, improved T_H17 differentiation, cured mucocutaneous candidiasis, and maintained remission of associated autoimmunity[41, 42]. The studies herein extend the usage of JAK inhibitors in primary atopic disorders by establishing disease control in STAT6 GOF disease. However, long-term data

regarding the outcome of this targeted therapy are needed to understand the full efficacy of these drugs in controlling the disease symptoms.

Finally, the identification of STAT6 GOF mutations as a cause of severe allergic dysregulation expands our knowledge of the genetic architecture of allergic diseases[1, 12, 67–70], and highlights the pivotal role of the IL-4/IL-13/IL4R/STAT6 axis in disease pathogenesis. Establishing the molecular underpinning of these diseases enables the use of targeted therapies to reverse the atopic inflammation and restore immune homeostasis in these patients[21, 71].

Supplementary Material

Refer to Web version on PubMed Central for supplementary material.

Acknowledgements:

Dr. Chatila received grant support from the National Institutes of Health (NIH R01AI128976 and R01AI126915). Dr. Baris obtained a grant from Scientific and Technological Research Council of Turkey (318S202). M.B is a recipient of a grant from the Office of Faculty Development at Boston Children's Hospital. We thank Drs. Hans Oettgen and Cynthia Kanagaratham for sharing reagents, and Melek Yorgun Altunbas for clinical support.

Abbreviations.

AD	Atopic dermatitis
APC	Allophycocyanin
CRTH2	Chemoattractant receptor homologous molecule expressed on TH2-type cells
cT_{FH}	Circulating follicular helper T
GATA3	GATA binding protein 3
GFP	Green fluorescent protein
GOF	Gain-of-function
HIES	Hyper IgE syndrome
IEI	Inborn errors of immunity
IL-4R	IL-4 receptor
JAK	Janus kinase
Jakinibs	JAK inhibitors
p	Phosphorylated
SH2	Src homology 2
STAT	Signal transducer and activator of transcription

Treg	Regulatory T
WES	Whole-exome sequencing
WT	Wild type

References

1. Nelson RW, Geha RS, McDonald DR. Inborn Errors of the Immune System Associated With Atopy. Front Immunol 2022; 13:860821. [PubMed: 35572516]
2. Vaseghi-Shanjani M, Snow AL, Margolis DJ, Latrous M, Milner JD, Turvey SE, et al. Atopy as Immune Dysregulation: Offender Genes and Targets. J Allergy Clin Immunol Pract 2022; 10:1737–56. [PubMed: 35680527]
3. Holland SM, DeLeo FR, Elloumi HZ, Hsu AP, Uzel G, Brodsky N, et al. STAT3 mutations in the hyper-IgE syndrome. N Engl J Med 2007; 357:1608–19. [PubMed: 17881745]
4. Zhang Q, Davis JC, Lamborn IT, Freeman AF, Jing H, Favreau AJ, et al. Combined immunodeficiency associated with DOCK8 mutations. N Engl J Med 2009; 361:2046–55. [PubMed: 19776401]
5. Engelhardt KR, McGhee S, Winkler S, Sassi A, Woellner C, Lopez-Herrera G, et al. Large deletions and point mutations involving the dedicator of cytokinesis 8 (DOCK8) in the autosomal-recessive form of hyper-IgE syndrome. J Allergy Clin Immunol 2009; 124:1289–302 e4. [PubMed: 20004785]
6. Bergerson JRE, Freeman AF. An Update on Syndromes with a Hyper-IgE Phenotype. Immunol Allergy Clin North Am 2019; 39:49–61. [PubMed: 30466772]
7. Bousfiha A, Jeddane L, Picard C, Al-Herz W, Ailal F, Chatila T, et al. Human Inborn Errors of Immunity: 2019 Update of the IUIS Phenotypical Classification. J Clin Immunol 2020; 40:66–81. [PubMed: 32048120]
8. Tangye SG, Al-Herz W, Bousfiha A, Cunningham-Rundles C, Franco JL, Holland SM, et al. Human Inborn Errors of Immunity: 2022 Update on the Classification from the International Union of Immunological Societies Expert Committee. J Clin Immunol 2022.
9. Lyons JJ, Milner JD. The clinical and mechanistic intersection of primary atopic disorders and inborn errors of growth and metabolism. Immunol Rev 2019; 287:135–44. [PubMed: 30565252]
10. Al Khatib S, Keles S, Garcia-Lloret M, Karakoc-Aydiner E, Reisli I, Artac H, et al. Defects along the T(H)17 differentiation pathway underlie genetically distinct forms of the hyper IgE syndrome. J Allergy Clin Immunol 2009; 124:342–8, 8 e1–5. [PubMed: 19577286]
11. Lyons JJ, Milner JD. Primary atopic disorders. J Exp Med 2018; 215:1009–22. [PubMed: 29549114]
12. Vaseghi-Shanjani M, Smith KL, Sara RJ, Modi BP, Branch A, Sharma M, et al. Inborn errors of immunity manifesting as atopic disorders. J Allergy Clin Immunol 2021; 148:1130–9. [PubMed: 34428518]
13. Milner JD, Vogel TP, Forbes L, Ma CA, Stray-Pedersen A, Niemela JE, et al. Early-onset lymphoproliferation and autoimmunity caused by germline STAT3 gain-of-function mutations. Blood 2015; 125:591–9. [PubMed: 25359994]
14. Kasap N, Aslan K, Karakurt LT, Bozkurt H, Canatan H, Cavkaytar O, et al. A novel gain-of-function mutation in STAT5B is associated with treatment-resistant severe atopic dermatitis. Clin Exp Allergy 2022.
15. Del Bel KL, Ragotte RJ, Saferali A, Lee S, Vercauteren SM, Mostafavi SA, et al. JAK1 gain-of-function causes an autosomal dominant immune dysregulatory and hypereosinophilic syndrome. J Allergy Clin Immunol 2017; 139:2016–20 e5. [PubMed: 28111307]
16. Liu L, Okada S, Kong XF, Kreins AY, Cypowyj S, Abhyankar A, et al. Gain-of-function human STAT1 mutations impair IL-17 immunity and underlie chronic mucocutaneous candidiasis. J Exp Med 2011; 208:1635–48. [PubMed: 21727188]
17. Hou J, Schindler U, Henzel WJ, Ho TC, Brasseur M, McKnight SL. An interleukin-4-induced transcription factor: IL-4 Stat. Science 1994; 265:1701–6. [PubMed: 8085155]

18. Takeda K, Tanaka T, Shi W, Matsumoto M, Minami M, Kashiwamura S, et al. Essential role of Stat6 in IL-4 signalling. Nature 1996; 380:627–30. [PubMed: 8602263]
19. Kaplan MH, Schindler U, Smiley ST, Grusby MJ. Stat6 is required for mediating responses to IL-4 and for development of Th2 cells. Immunity 1996; 4:313–9. [PubMed: 8624821]
20. Nelms K, Keegan AD, Zamorano J, Ryan JJ, Paul WE. The IL-4 receptor: signaling mechanisms and biologic functions. Annu Rev Immunol 1999; 17:701–38. [PubMed: 10358772]
21. Harb H, Chatila TA. Mechanisms of Dupilumab. Clin Exp Allergy 2020; 50:5–14. [PubMed: 31505066]
22. Luo Y, Alexander M, Gadina M, O'Shea JJ, Meylan F, Schwartz DM. JAK-STAT signaling in human disease: From genetic syndromes to clinical inhibition. J Allergy Clin Immunol 2021; 148:911–25. [PubMed: 34625141]
23. Levy DE, Darnell JE Jr. Stats: transcriptional control and biological impact. Nat Rev Mol Cell Biol 2002; 3:651–62. [PubMed: 12209125]
24. Schindler C, Darnell JE Jr. Transcriptional responses to polypeptide ligands: the JAK-STAT pathway. Annu Rev Biochem 1995; 64:621–51. [PubMed: 7574495]
25. Wang W, Wang L, Zha B. The roles of STAT6 in regulating B cell fate, activation, and function. Immunol Lett 2021; 233:87–91. [PubMed: 33662403]
26. Palm NW, Rosenstein RK, Medzhitov R. Allergic host defences. Nature 2012; 484:465–72. [PubMed: 22538607]
27. Pulendran B, Artis D. New paradigms in type 2 immunity. Science 2012; 337:431–5. [PubMed: 22837519]
28. Scheinman EJ, Avni O. Transcriptional regulation of GATA3 in T helper cells by the integrated activities of transcription factors downstream of the interleukin-4 receptor and T cell receptor. J Biol Chem 2009; 284:3037–48. [PubMed: 19056736]
29. Maier E, Duschl A, Horejs-Hoeck J. STAT6-dependent and -independent mechanisms in Th2 polarization. Eur J Immunol 2012; 42:2827–33. [PubMed: 23041833]
30. Pillemer BB, Qi Z, Melgert B, Oriss TB, Ray P, Ray A. STAT6 activation confers upon T helper cells resistance to suppression by regulatory T cells. J Immunol 2009; 183:155–63. [PubMed: 19535633]
31. Noval Rivas M, Burton OT, Wise P, Charbonnier LM, Georgiev P, Oettgen HC, et al. Regulatory T cell reprogramming toward a Th2-cell-like lineage impairs oral tolerance and promotes food allergy. Immunity 2015; 42:512–23. [PubMed: 25769611]
32. Hancock DB, Romieu I, Chiu GY, Sienra-Monge JJ, Li H, Estela Del Rio-Navarro B, et al. STAT6 and LRP1 polymorphisms are associated with food allergen sensitization in Mexican children. J Allergy Clin Immunol 2012; 129:1673–6. [PubMed: 22534531]
33. O'Shea JJ, Schwartz DM, Villarino AV, Gadina M, McInnes IB, Laurence A. The JAK-STAT pathway: impact on human disease and therapeutic intervention. Annu Rev Med 2015; 66:311–28. [PubMed: 25587654]
34. Yildiz M, Li H, Bernard D, Amin NA, Ouillette P, Jones S, et al. Activating STAT6 mutations in follicular lymphoma. Blood 2015; 125:668–79. [PubMed: 25428220]
35. von Hoff L, Kargel E, Franke V, McShane E, Schulz-Beiss KW, Patone G, et al. Autocrine LTA signaling drives NF-kappaB and JAK-STAT activity and myeloid gene expression in Hodgkin lymphoma. Blood 2019; 133:1489–94. [PubMed: 30696620]
36. Bruns HA, Schindler U, Kaplan MH. Expression of a constitutively active Stat6 in vivo alters lymphocyte homeostasis with distinct effects in T and B cells. J Immunol 2003; 170:3478–87. [PubMed: 12646608]
37. Sehra S, Bruns HA, Ahyi AN, Nguyen ET, Schmidt NW, Michels EG, et al. IL-4 is a critical determinant in the generation of allergic inflammation initiated by a constitutively active Stat6. J Immunol 2008; 180:3551–9. [PubMed: 18292582]
38. Kolukisa B, Baser D, Akcam B, Danielson J, Bilgic Eltan S, Haliloglu Y, et al. Evolution and long-term outcomes of combined immunodeficiency due to CARMIL2 deficiency. Allergy 2021.
39. Kiykim A, Ogulur I, Dursun E, Charbonnier LM, Nain E, Cekic S, et al. Abatacept as a Long-Term Targeted Therapy for LRBA Deficiency. J Allergy Clin Immunol Pract 2019; 7:2790–800 e15. [PubMed: 31238161]

40. Baris S, Alroqi F, Kiykim A, Karakoc-Aydiner E, Ogulur I, Ozen A, et al. Severe Early-Onset Combined Immunodeficiency due to Heterozygous Gain-of-Function Mutations in STAT1. J Clin Immunol 2016; 36:641–8. [PubMed: 27379765]
41. Kayaoglu B, Kasap N, Yilmaz NS, Charbonnier LM, Geckin B, Akcay A, et al. Stepwise Reversal of Immune Dysregulation Due to STAT1 Gain-of-Function Mutation Following Ruxolitinib Bridge Therapy and Transplantation. J Clin Immunol 2021.
42. Weinacht KG, Charbonnier LM, Alroqi F, Plant A, Qiao Q, Wu H, et al. Ruxolitinib reverses dysregulated T helper cell responses and controls autoimmunity caused by a novel signal transducer and activator of transcription 1 (STAT1) gain-of-function mutation. J Allergy Clin Immunol 2017; 139:1629–40 e2. [PubMed: 28139313]
43. Cui Y, Benamar M, Schmitz-Abe K, Poondi-Krishnan V, Chen Q, Jugder BE, et al. A Stk4-Foxp3-NF-kappaB p65 transcriptional complex promotes T(reg) cell activation and homeostasis. Sci Immunol 2022; 7:eabl8357.
44. Schmitz-Abe K, Li Q, Rosen SM, Nori N, Madden JA, Genetti CA, et al. Unique bioinformatic approach and comprehensive reanalysis improve diagnostic yield of clinical exomes. Eur J Hum Genet 2019; 27:1398–405. [PubMed: 30979967]
45. Severity scoring of atopic dermatitis: the SCORAD index. Consensus Report of the European Task Force on Atopic Dermatitis. Dermatology 1993; 186:23–31. [PubMed: 8435513]
46. Grimbacher B, Schaffer AA, Holland SM, Davis J, Gallin JI, Malech HL, et al. Genetic linkage of hyper-IgE syndrome to chromosome 4. Am J Hum Genet 1999; 65:735–44. [PubMed: 10441580]
47. Tate JG, Bamford S, Jubb HC, Sondka Z, Beare DM, Bindal N, et al. COSMIC: the Catalogue Of Somatic Mutations In Cancer. Nucleic Acids Res 2019; 47:D941–D7. [PubMed: 30371878]
48. Chen Y, Lu H, Zhang N, Zhu Z, Wang S, Li M. PremPS: Predicting the impact of missense mutations on protein stability. PLoS Comput Biol 2020; 16:e1008543. [PubMed: 33378330]
49. Faletti L, Ehl S, Heeg M. Germline STAT3 gain-of-function mutations in primary immunodeficiency: Impact on the cellular and clinical phenotype. Biomed J 2021; 44:412–21. [PubMed: 34366294]
50. Li J, Rodriguez JP, Niu F, Pu M, Wang J, Hung LW, et al. Structural basis for DNA recognition by STAT6. Proc Natl Acad Sci U S A 2016; 113:13015–20. [PubMed: 27803324]
51. Vercelli D, Jabara HH, Lee BW, Woodland N, Geha RS, Leung DY. Human recombinant interleukin 4 induces Fc epsilon R2/CD23 on normal human monocytes. J Exp Med 1988; 167:1406–16. [PubMed: 2965737]
52. Jabara HH, Fu SM, Geha RS, Vercelli D. CD40 and IgE: synergism between anti-CD40 monoclonal antibody and interleukin 4 in the induction of IgE synthesis by highly purified human B cells. J Exp Med 1990; 172:1861–4. [PubMed: 1701824]
53. Elo LL, Jarvenpaa H, Tuomela S, Raghav S, Ahlfors H, Laurila K, et al. Genome-wide profiling of interleukin-4 and STAT6 transcription factor regulation of human Th2 cell programming. Immunity 2010; 32:852–62. [PubMed: 20620947]
54. Van Dyken SJ, Locksley RM. Interleukin-4- and interleukin-13-mediated alternatively activated macrophages: roles in homeostasis and disease. Annu Rev Immunol 2013; 31:317–43. [PubMed: 23298208]
55. Schubart C, Krljanac B, Otte M, Symowski C, Martini E, Gunther C, et al. Selective expression of constitutively activated STAT6 in intestinal epithelial cells promotes differentiation of secretory cells and protection against helminths. Mucosal Immunol 2019; 12:413–24. [PubMed: 30446727]
56. Liang HE, Reinhardt RL, Bando JK, Sullivan BM, Ho IC, Locksley RM. Divergent expression patterns of IL-4 and IL-13 define unique functions in allergic immunity. Nat Immunol 2011; 13:58–66. [PubMed: 22138715]
57. Burton OT, Darling AR, Zhou JS, Noval-Rivas M, Jones TG, Gurish MF, et al. Direct effects of IL-4 on mast cells drive their intestinal expansion and increase susceptibility to anaphylaxis in a murine model of food allergy. Mucosal Immunol 2013; 6:740–50. [PubMed: 23149659]
58. Chapoval S, Dasgupta P, Dorsey NJ, Keegan AD. Regulation of the T helper cell type 2 (Th2)/T regulatory cell (Treg) balance by IL-4 and STAT6. J Leukoc Biol 2010; 87:1011–8. [PubMed: 20335310]

59. Tachdjian R, Al Khatib S, Schwinglshackl A, Kim HS, Chen A, Blasioli J, et al. In vivo regulation of the allergic response by the IL-4 receptor alpha chain immunoreceptor tyrosine-based inhibitory motif. J Allergy Clin Immunol 2010; 125:1128–36 e8. [PubMed: 20392476]
60. Massoud AH, Charbonnier LM, Lopez D, Pellegrini M, Phipatanakul W, Chatila TA. An asthma-associated IL4R variant exacerbates airway inflammation by promoting conversion of regulatory T cells to TH17-like cells. Nat Med 2016; 22:1013–22. [PubMed: 27479084]
61. Noval Rivas M, Burton OT, Oettgen HC, Chatila T. IL-4 production by group 2 innate lymphoid cells promotes food allergy by blocking regulatory T-cell function. J Allergy Clin Immunol 2016; 138:801–11 e9. [PubMed: 27177780]
62. Gadina M, Johnson C, Schwartz D, Bonelli M, Hasni S, Kanno Y, et al. Translational and clinical advances in JAK-STAT biology: The present and future of jakinibs. J Leukoc Biol 2018; 104:499–514. [PubMed: 29999544]
63. Forbes LR, Vogel TP, Cooper MA, Castro-Wagner J, Schussler E, Weinacht KG, et al. Jakinibs for the treatment of immune dysregulation in patients with gain-of-function signal transducer and activator of transcription 1 (STAT1) or STAT3 mutations. J Allergy Clin Immunol 2018; 142:1665–9. [PubMed: 30092289]
64. Balci S, Ekinci RMK, de Jesus AA, Goldbach-Mansky R, Yilmaz M. Baricitinib experience on STING-associated vasculopathy with onset in infancy: A representative case from Turkey. Clin Immunol 2020; 212:108273. [PubMed: 31626957]
65. Hadjadj J, Castro CN, Tusseau M, Stolzenberg MC, Mazerolles F, Aladjidi N, et al. Early-onset autoimmunity associated with SOCS1 haploinsufficiency. Nat Commun 2020; 11:5341. [PubMed: 33087723]
66. Eisenberg R, Gans MD, Leahy TR, Gothe F, Perry C, Raffeld M, et al. JAK inhibition in early-onset somatic, nonclonal STAT5B gain-of-function disease. J Allergy Clin Immunol Pract 2021; 9:1008–10 e2. [PubMed: 33290916]
67. Vercelli D Discovering susceptibility genes for asthma and allergy. Nat Rev Immunol 2008; 8:169–82. [PubMed: 18301422]
68. Milner JD. Primary Atopic Disorders. Annu Rev Immunol 2020; 38:785–808. [PubMed: 32126183]
69. Gupta J, Johansson E, Bernstein JA, Chakraborty R, Khurana Hershey GK, Rothenberg ME, et al. Resolving the etiology of atopic disorders by using genetic analysis of racial ancestry. J Allergy Clin Immunol 2016; 138:676–99. [PubMed: 27297995]
70. SoRelle JA, Chen Z, Wang J, Yue T, Choi JH, Wang KW, et al. Dominant atopy risk mutations identified by mouse forward genetic analysis. Allergy 2021; 76:1095–108. [PubMed: 32810290]
71. Shankar A, McAlees JW, Lewkowich IP. Modulation of IL-4/IL-13 cytokine signaling in the context of allergic disease. J Allergy Clin Immunol 2022; 150:266–76. [PubMed: 35934680]

Key messages.

1. A germline STAT6 gain-of-function mutation gave rise to severe allergic inflammation.
2. Therapy with a Janus kinase inhibitor controlled disease manifestations and suppressed the associated immune dysregulation.

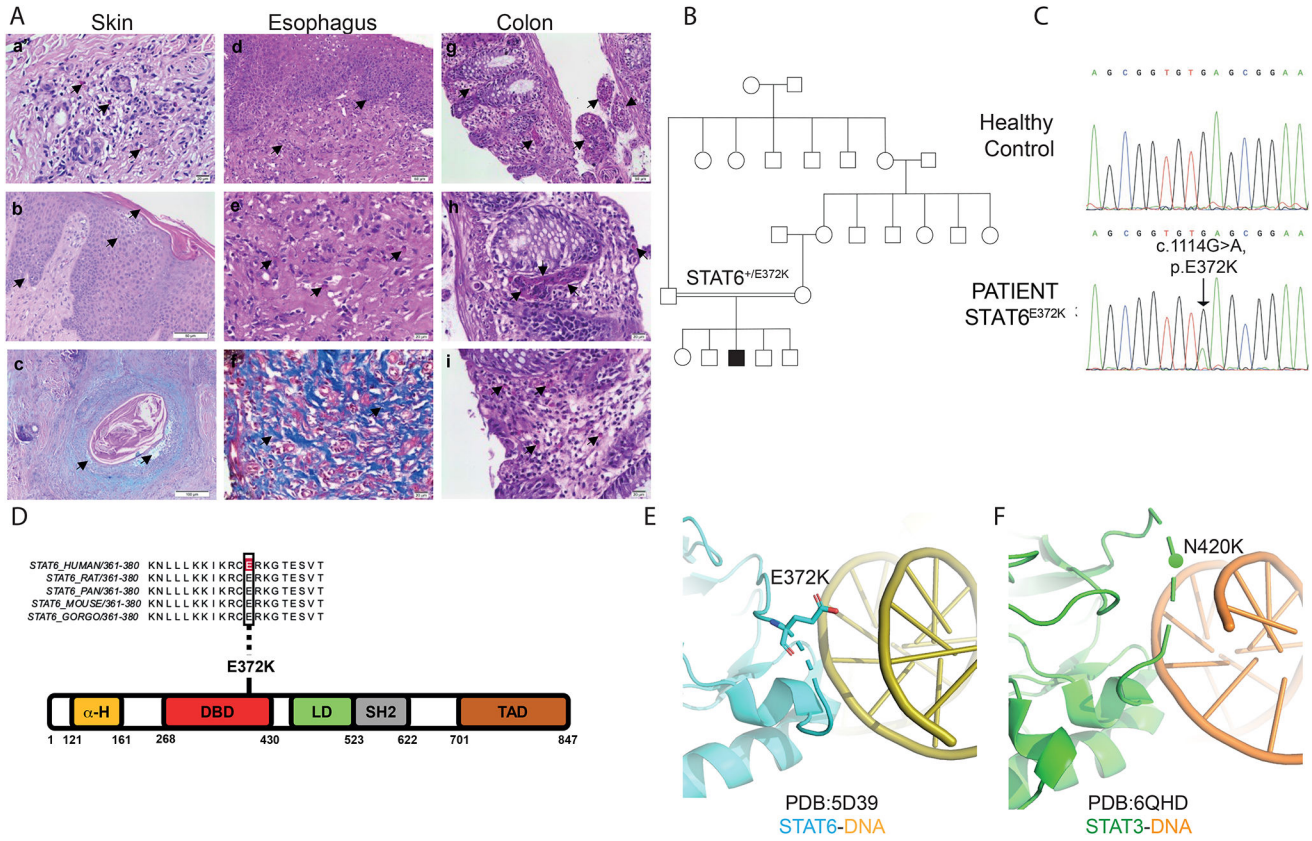

Figure 1. Identification of a STAT6^{E372K} mutation in a child with severe allergy dysregulation.

(A) Scattered eosinophils in dermis, hematoxylin and eosin staining (H&E), 40X **(a).** Parakeratosis, spongiosis and acanthosis of epidermis (black arrows), H&E, 20X **(b).** Mucin accumulation dissociating epithelial cells of follicular epithelium, dilatation of follicle (black arrows), periodic acid schiff and Alcian Blue 2.5 staining, 10X **(c).** Gastrointestinal pathology shows esophagitis and scattered eosinophils with marked fibrosis in the subepithelial area of the esophagus (black arrows), H&E; 20X, 40X and trichrome staining; 40X, respectively **(d, e, f)**. Inflammation with eosinophils in lamina propria, intraepithelial and intravascular areas of sigmoid colon, (H&E); 20X, 40X, 40X, respectively **(g, h, i)**. **(B)** Pedigree of STAT6 GOF patient. Double lines indicate consanguinity; a filled black square depicts the patient. Males and females are distinguished by squares and circles, respectively. **(C)** Sanger sequencing analysis of the *STAT6* c.1114G>A mutation in the index patient versus a healthy control. **(D)** Schematic diagram of STAT6 protein domains. The depicted domains are the α-Helix domain (α-H), DNA binding domain (DBD), linker domain (LD), SH2 Src homology 2 domain (SH2), and a transactivation domain (TAD). The heterozygous mutation localizes to the DBD. Multiple sequence alignment analysis of STAT6 proteins of different species demonstrates conservation of the STAT6E372 residue. **(E, F)** Structural modeling of the interaction of the STAT6^{E372K} and STAT3^{N420K} with DNA.

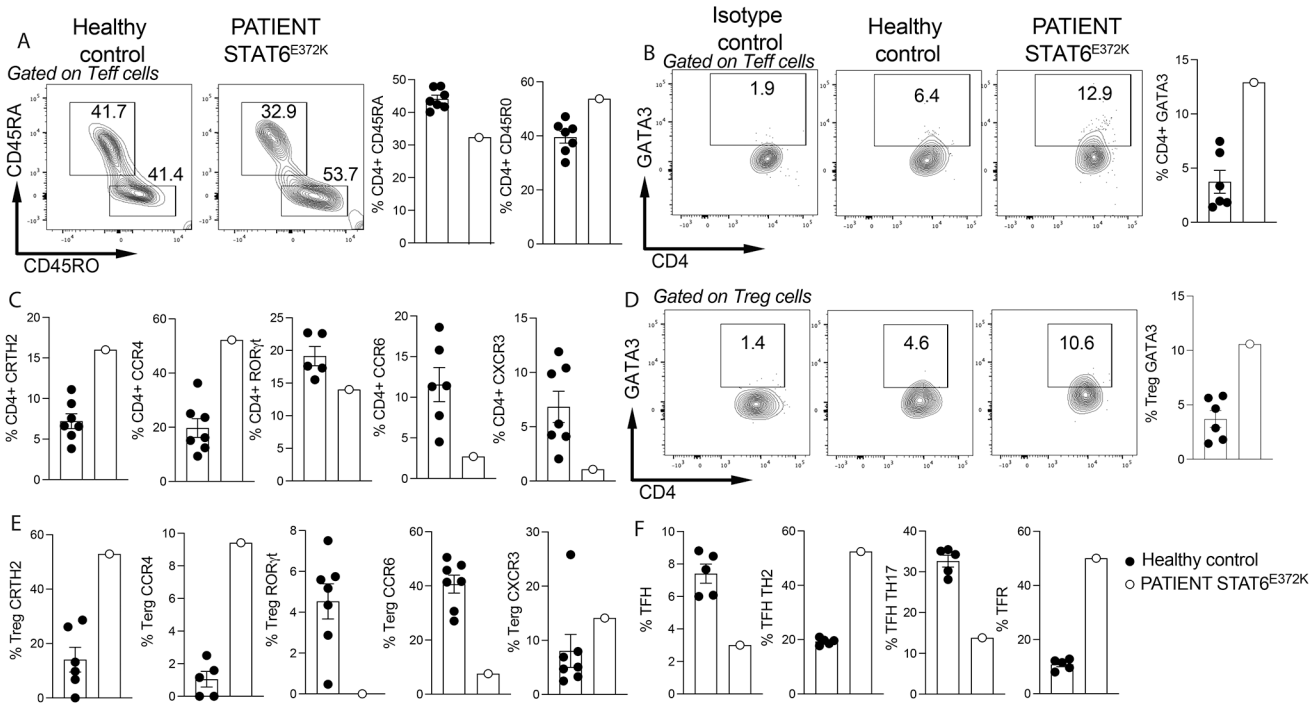

Figure 2. The STAT6^{E372K} mutation is associated with skewed T_H2 responses.

(A) Flow cytometric analysis and graphical representation of naïve ($CD3^+CD4^+CD45RO^-CD45RA^+$) and memory ($CD3^+CD4^+CD45RO^+CD45RA^-$) Teff cells in Healthy controls and the patient with STAT6^{E372K} mutation. (**B)** Flow cytometric analysis and graphical representation of T_H2 cells ($CD3^+CD4^+GATA3^+$) in the respective groups. **(C)** Cells frequencies of $CD4^+CRTH2^+$, $CD4^+CCR4^+$, $CD4^+ROR\gamma^+$, $CD4^+CCR6^+$, $CD4^+CXCR3^+$ T cells in the respective groups. **(D)** Flow cytometric analysis and graphical representation of Treg GATA3$^+$ cells ($CD3^+CD4^+CD127^-Foxp3^+GATA3^+$) in the respective groups. **(E)** Cells frequencies of Treg $CRTH2^+$, Treg $CCR4^+$, Treg $ROR\gamma T^+$, Treg $CCR6^+$, and Treg $CXCR3^+$ T cells in the respective groups. **(F)** Cells frequencies of circulating T follicular helper (cT_{FH}), T follicular helper T_H2 ($CD4^+CXCR5^+CD45RA^-CXCR3^-CCR6^-$), T follicular helper T_H17 ($CD4^+CXCR5^+CD45RA^-CXCR3^-CCR6^+$), and T follicular regulatory cells in the respective groups. Each symbol represents one subject. Numbers in flow plots indicate percentages. Error bars indicate SEM.

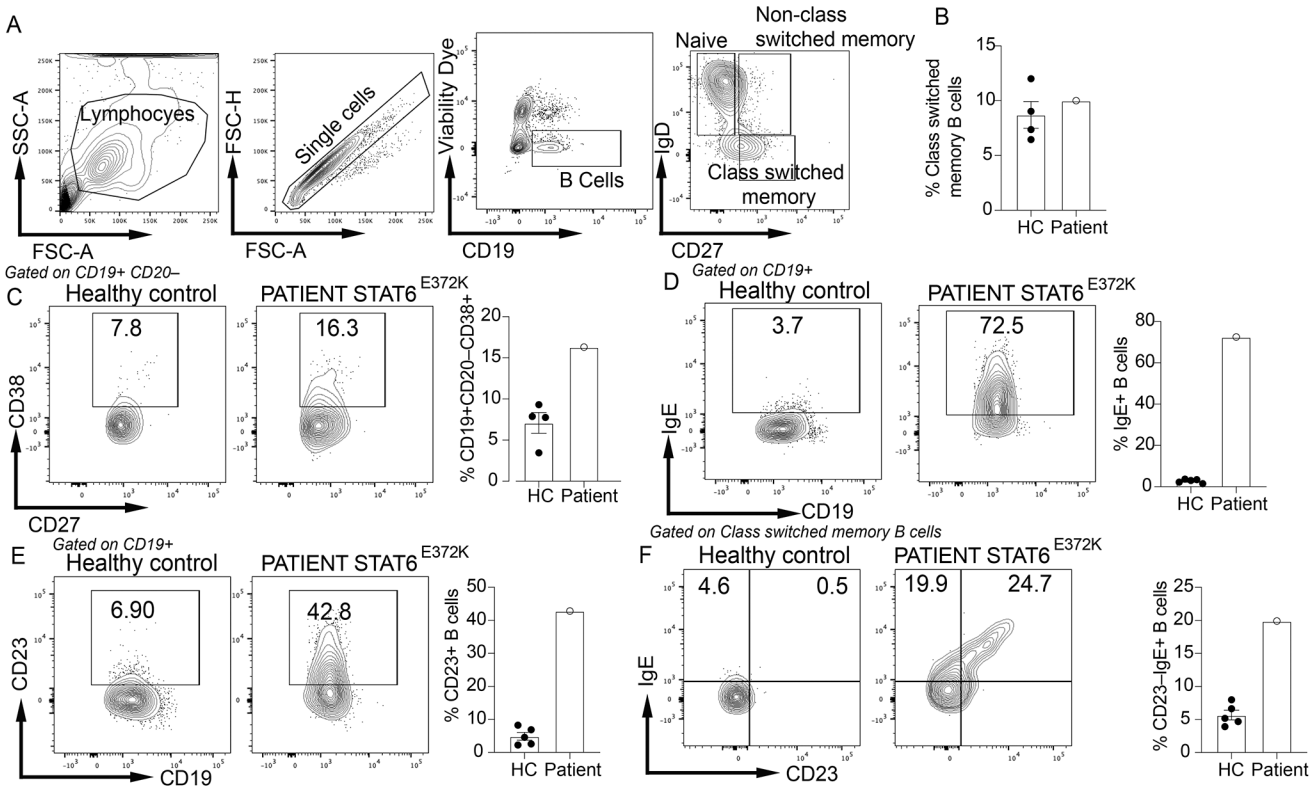

Figure 3. The STAT6^{E372K} mutation is associated with increased circulating CD23^{+} and IgE^{+} memory B cells.

(A) Gating strategy for B cells analysis**. (B)** Cell Frequencies of Class switched memory B cells (CD19^{+}, CD27^{+} IgD$^{–}$). (**C**) Flow cytometric analysis and graphical representation of Plasmablasts (CD19^{+} CD20$^{–}$ CD38^{+}) in healthy controls and in the patient with STAT6^{E372K} mutation. **(D)** Flow cytometric analysis and graphical representation of IgE^{+} circulating B cells in healthy controls and in the patient with the STAT6^{E372K} mutation. **(E, F)** Flow cytometric analysis and graphical representation of CD23^{+} **(E)** and CD23–IgE+ memory (IgD$^{–}$ CD27^{+}) B cells **(F)** in healthy controls and in the patient with STAT6^{E372K} mutation. Each symbol represents one subject. Numbers in flow plots indicate percentages. Error bars indicate SEM.

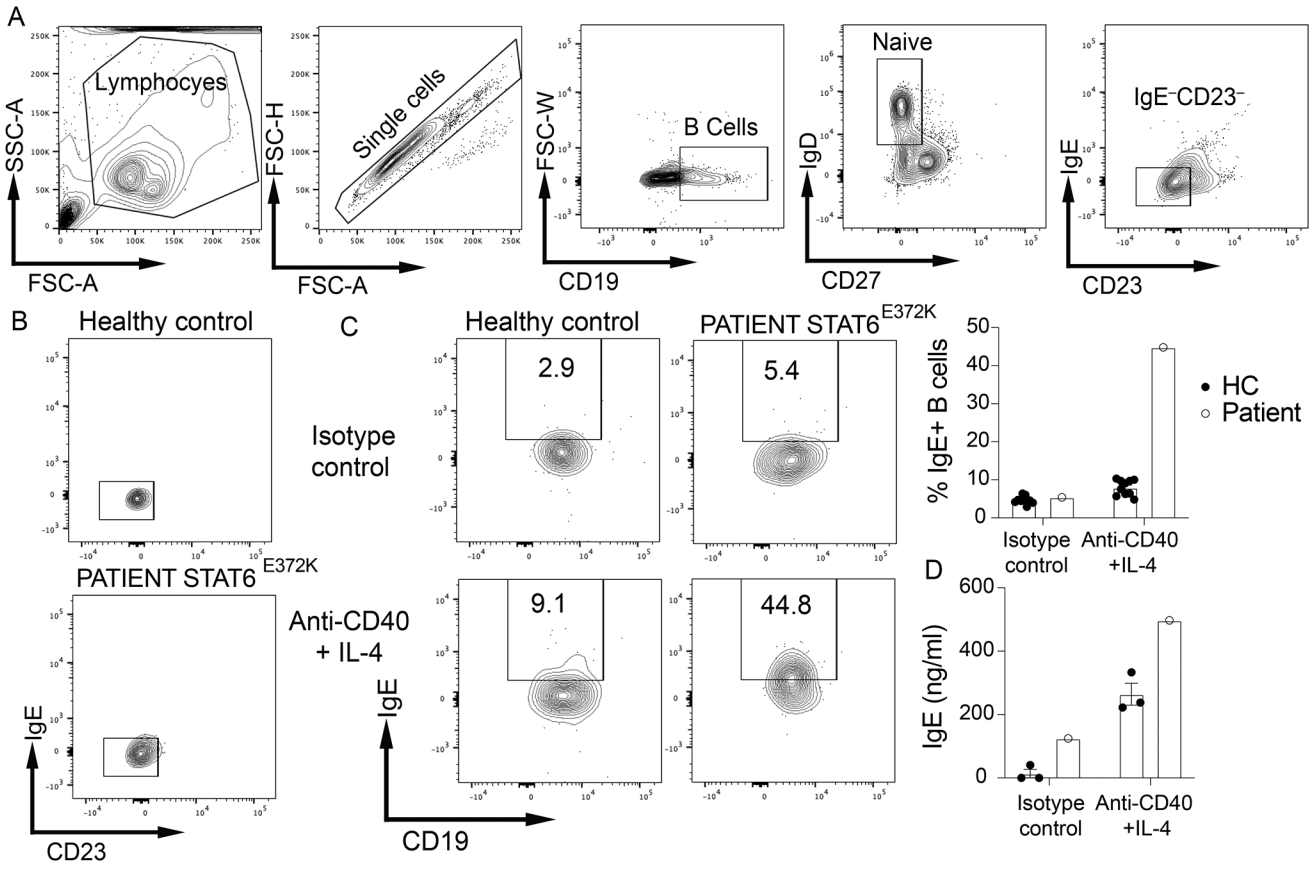

Figure 4. The STAT6^{E372K} mutation is associated with enhanced B cell class switching to IgE.

(A) Gating strategy for cell-sorting of naïve B cells ($CD19^+IgD^+CD27^-CD23^-IgE^-$). **(B)** Purity check after cell sorting. **(C, D)** Flow cytometric analysis, frequencies of IgE^+ B cells (C), and total IgE in the culture supernatants (D) in cultures of the respective sorted B cell populations that were treated with an isotype control mAb or with anti-CD40 mAb+IL-4. Each symbol represents one subject. Numbers in flow plots indicate percentages. Error bars indicate SEM.

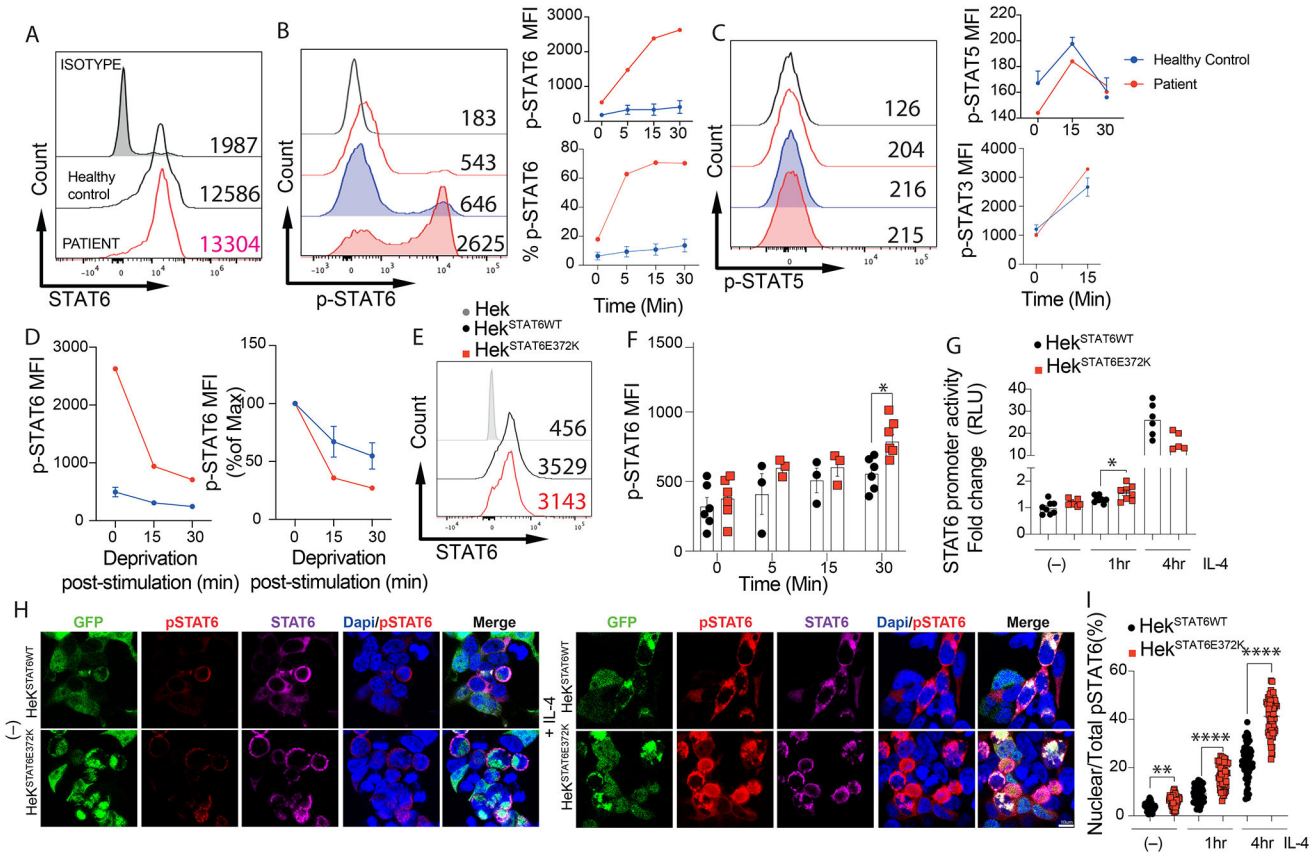

Figure 5. STAT6^{E372K} is a GOF mutation.

(A) Flow cytometric analysis and mean fluorescence intensity (MFI) of STAT6 in CD4^{+} T cells of Healthy controls and the patient with STAT6^{E372K} mutation. **(B)** Flow cytometric analysis and MFI of p-STAT6 (top) and frequencies of p-STAT6 cells (bottom) in CD4^{+} T cells of Healthy controls and the patient with STAT6^{E372K} mutation after stimulation with IL-4 (20ng/ml) for 5 to 30 minutes (Black line: Healthy control unstimulated, Red line: STAT6^{E372K} patient unstimulated, Blue: Healthy control stimulated with IL-4 and Red: STAT6^{E372K} patient stimulated with IL-4). **(C)** Flow cytometric analysis and MFI of p-STAT5 (top) and of p-STAT3 (bottom) in CD4^{+} T cells of Healthy controls and the patient with STAT6^{E372K} mutation after stimulation with IL-2 (20ng/ml) or IL-6 (20ng/ml), respectively for 5 to 30 minutes **(D)** Dephosphorylation kinetics of phospho-STAT6 in response to deprivation of IL-4 and in CD4^{+} T cells represented as absolute MFI (left) and normalized to maximum expression before deprivation (right). **(E)** MFI expression of STAT6 in HEK293 cell transfected with either STAT6^{WT} or STAT6^{E372K} proteins. **(F)** MFI expression of p-STAT6 in HEK293 cell transfected with either STAT6^{WT} or STAT6^{E372K} proteins after IL-4 (20ng/ml) stimulation for 5 to 30 minutes. **(G)** STAT6 response element-driven luciferase reporter activation by STAT6^{WT} or STAT6^{E372K} transfected into HEK293 cells at baseline and following IL-4 treatment for 1 and 4 hr. RLU: Relative Luciferase Unit. **(H, I)** Confocal microscopic analysis of total STAT6, p-STAT6 and DAPI in HEK293 cells transfected with either STAT6^{WT} or STAT6^{E372K} and then either sham-treated or stimulated with IL-4 for 1 and 4 hr, respectively. Numbers in flow plots indicate MFI. Error bars

indicate SEM. Statistical tests: *P<0.05, **P<0.01, ****P<0.0001 by two-way ANOVA with Dunnett's post hoc analysis **(F; G, I)**.

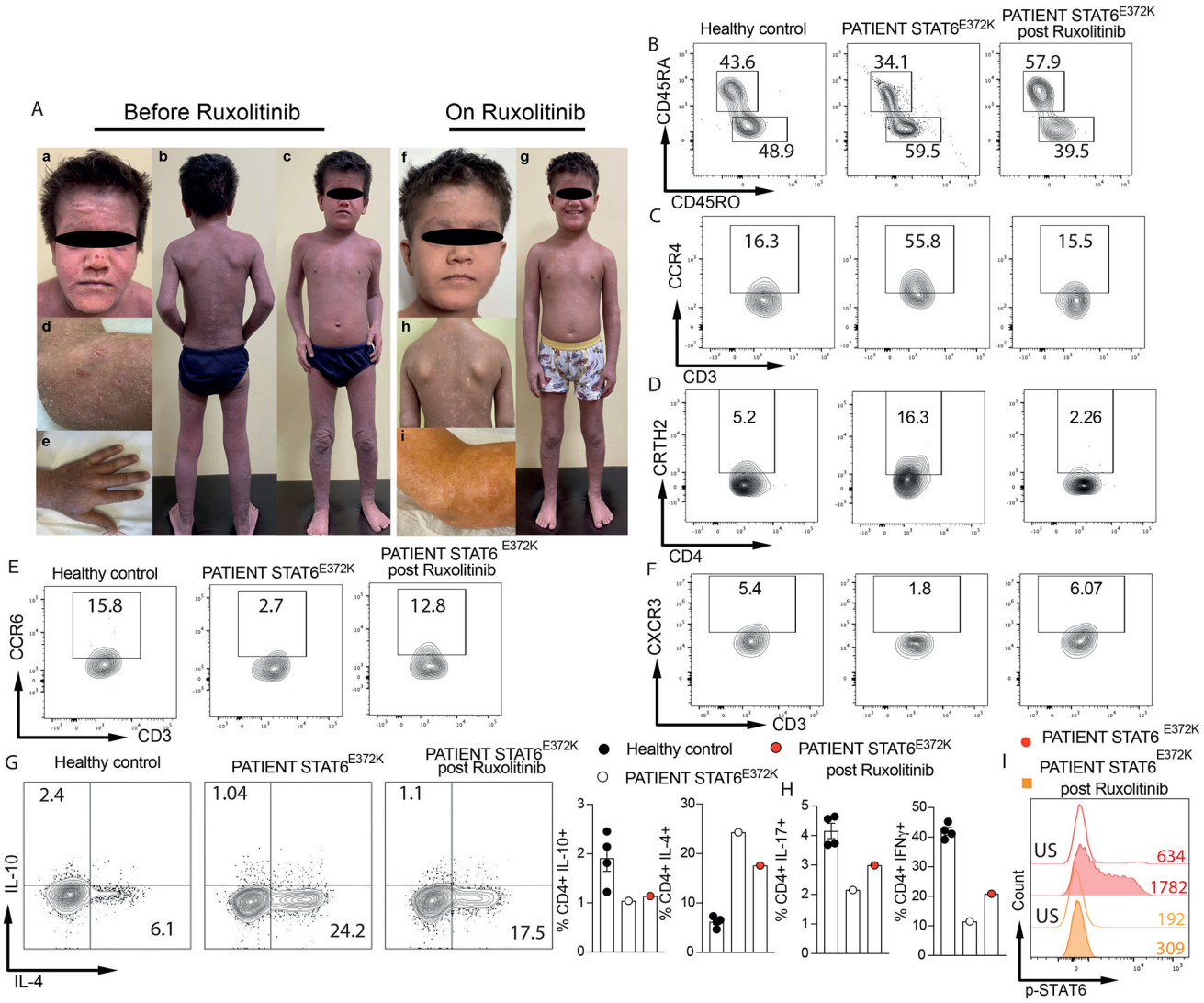

Figure 6. Ruxolitinib therapy suppresses the allergic dysregulation and inhibits the T_H2 skewing and STAT6 hyperactivation.

(A) Response of patient atopic dermatitis to ruxolitinib therapy. **(a-e),** Severe atopic dermatitis before ruxolitinib therapy covering the face (a), body (b, c), elbow and hand (d, e) of the patient. **(f-i)**, control of atopic dermatitis after ruxolitinib treatment. **(B)** Flow cytometric analysis of naïve ($CD3^+CD4^+CD45RO^-CD45RA^+$) and memory ($CD3^+CD4^+CD45RO^+CD45RA^-$) Teff cells in healthy controls and the patient with $STAT6^{E372K}$ mutation pre- and post-therapy with ruxolitinib. **(C, D)** Flow cytometric analysis of $CD4^+CCR4^+$**(C)** and $CD4^+CRTH2^+$**(D)** T cells in the respective groups. **(E, F)** Cells frequencies of $CD4^+CCR6^+$**(E)** and $CD4^+CXCR3^+$**(F)** T cells in the respective groups. **(G, H)** Flow cytometric analysis with representative plots of IL-4-, IL-17-, IFN-γ- and IL-10-producing circulating $CD4^+$ T cells pre-and post-ruxolitinib therapy compared with healthy controls. **(I)** Flow cytometric analysis and MFI of p-STAT6 (left) and p-STAT6 fold change (right) in $CD4^+$ T cells of healthy controls and the patient with $STAT6^{E372K}$ mutation pre- and post-treated with ruxolitinib after stimulation with IL-4 (20ng/ml)

for 5 to 30 minutes (Red line: $STAT6^{E372K}$ patient pre-treatment unstimulated, Red: $STAT6^{E372K}$ patient stimulated with IL-4, Orange line: $STAT6^{E372K}$ patient post-treatment with ruxolitinib and orange: $STAT6^{E372K}$ patient post-treated with ruxolitinib stimulated with IL-4). Each symbol represents one subject. Numbers in flow plots indicate percentages. Error bars indicate SEM.

Table 1.

Immunological evaluation of the patient with STAT6^{E372K} gain-of-function mutation.

Parameters	Before ruxolitinib			On ruxolitinib	Normal range for age
Age (yrs)	8	9	10	10	
Complete Blood Count					
Lymphocyte (/mm^3)	5,100	2,700	1,800	3,660	1,500–8,500
Neutrophil (/mm^3)	**9,600**	4,900	4,800	2,600	1,500–6,500
Eosinophil (/mm^3)	**3,100**	**2,130**	**1,140**	440	0–500
Hemoglobin (g/dl)	**9.5**	10.6	**8.6**	11.4	10–15.5
Thrombocyte (/mm^3)	**831,000**	**633,000**	167,000	492,000	150,000–450,000
Immunoglobulins and antibody responses					
IgG (mg/dl)	1610	1391	1803	1410	842–1953
IgA (mg/dl)	260	152	188	114	62–398
IgM (mg/dl)	116	178	173	109	54–392
IgE (IU/ml)	**44,626**	**50,000**	**39,700**	**37,550**	<50
Anti-Hbs (mIU/mL)	154	On IVIG	On IVIG	On IVIG	>10
Anti-Mumps (Index)	1.53	On IVIG	On IVIG	On IVIG	>1.1
Isohemagglutinin titer (Anti A-IgM)	1/256	On IVIG	On IVIG	On IVIG	≥1/8
Isohemagglutinin titer (Anti B-IgM)	1/64	On IVIG	On IVIG	On IVIG	≥1/8
Lymphocyte subsets (/mm^3)					
CD3$^+$T cells	**4,539**	2,268	1,585	3,100	1,214–4,130
CD3$^+$4$^+$T cells	**3,162**	1,674	1,200	2,340	607–2,110
CD3$^+$8$^+$T cells	1,224	540	325	640	380–2,084
CD19$^+$B cells	255	**120**	**80**	296	197–867
CD16$^+$56$^+$NK cells	255	126	90	114	111–963
CD4$^+$T-cell subsets (%)					
CD4$^+$CD45RA$^+$CCR7$^+$	61	NA	51	72	40–78
CD4$^+$CD45 RA$^-$C CR7$^+$	**11**	NA	**12**	**9**	17–53
CD4$^+$CD45 RA$^-$C CR7$^-$	**22**	NA	**30**	14	2–14
CD4$^+$CD45RA$^+$CCR7$^-$	5	NA	6	6	0–43
CD8$^+$T-cell subsets (%)					
CD8$^+$CD45RA$^+$CCR7$^+$	46	NA	53	77	22–67
CD8$^+$CD45RA$^-$CCR7$^+$	3	NA	3	7	1–10
CD8$^+$CD45RA$^-$CCR7$^-$	28	NA	25	9	6–41
CD8$^+$CD45RA$^+$CCR7$^-$	22	NA	18	6	18–74
CD19 cell subsets (%)					
CD19$^+$CD27$^-$IgD$^+$	69	NA	50	71	55–90
CD19$^+$CD27$^+$IgD$^+$	**6**	NA	7	7	7–31

Parameters	Before ruxolitinib			On ruxolitinib	Normal range for age
$CD19^{+}CD27^{+}IgD^{-}$	18	NA	25	12	2–52
$CD21^{low}CD3^{low}$B cells	11	NA	3	12	1–13
IgRT	-	400 mg/kg/per 3 weeks	400 mg/kg/per 3 weeks	400 mg/kg/per 3 weeks	
Antibacterial prophylaxis	-	TMP-SMX	TMP-SMX	TMP-SMX	
Antifungal prophylaxis	-	-	Fluconazole	-	
Antiviral prophylaxis	-	-	-	Aciclovir	

Abbreviations: Anti-Hbs: Anti-hepatitis B surface antibody, IgRT: Immunoglobulin replecment therapy, NA: Not-available; PHA: Phytohemagglutinin; TMP-SMX: Trimethoprim-sulfamethoxazole. Abnormal values are shown in a bold manner. $CD4^{+}$ naïve T cells ($CD4^{+}CD45RA^{+}CCR7^{+}$), central memory $CD4^{+}$ T cells ($CD4^{+}CD45RA^{-}CCR7^{+}$), effector memory $CD4^{+}$ T cells ($CD4^{+}CD45RA^{-}CCR7^{-}$), terminally differentiated effector memory $CD4^{+}$ T cells ($CD4^{+}CD45RA^{+}CCR7^{-}$), $CD8^{+}$ naive T cells ($CD8^{+}CD45RA^{+}CCR7^{+}$), central memory $CD8^{+}$ T cells ($CD8^{+}CD45RA^{-}CCR7^{+}$), effector memory $CD8^{+}$ T cells ($CD8^{+}CD45RA^{-}CCR7^{-}$), terminally differentiated effector memory $CD8^{+}$ T cells ($CD8^{+}CD45RA^{+}CCR7^{-}$), naive mature B cells ($CD19^{+}CD27^{-}IgD^{+}$), non-switched memory B cells ($CD19^{+}CD27^{+}IgD^{+}$), switched memory B cells ($CD19^{+}CD27^{+}IgD^{-}$), autoreactive B cells ($CD21^{low}CD3^{low}$).